Electronic Supplementary Material (ESI) for Dalton Transactions.
This journal is © The Royal Society of Chemistry 2024

Supporting Information

For

A series of viologen complexes containing thiophene and Br^- dual fluorescent chromophores for continuous visual sensing of pH and Hg^{2+}

College of Chemistry and Materials Engineering, Bohai University, Jinzhou 121013, P. R. China

**Corresponding authors E-mail: ying@bhu.edu.cn. wangxiuli@bhu.edu.cn*

Experimental section

Instrumentation

Powder X-ray diffraction (PXRD) was measured using an Ultima IV X-ray powder diffractometer (Kurary, Tokyo, Japan) at 40 kV and 40 mA using Cu Kα radiation (k = 1.5406 Å). Ultraviolet-visible absorption spectra and fluorescence spectra of the as-prepared products were performed by a Shimadzu UV-2600 spectrophotometer and Perkin-Elmer luminescence spectrometer (LS-55). Fourier transform infrared spectroscopy (FTIR) was used to identify the functional groups of the products by a Shimadzu IRAffinity 1S spectrophotometer. X-ray photoelectron spectroscopy (XPS) measurement for elemental component analysis of the production was conducted by an ESCALAB 250Xi X-ray photoelectron spectrometer. The single crystal X-ray was measured on a Bruker APEX-IV CCD diffractometer with graphite monochromatic Mo Ka radiation at 298 K, and the structure was solved by direct method and refined with the full matrix least-squares method on F^2 embedded in SHELXTL program through using the Olex2 as the graphical interface. All hydrogen atoms were placed geometrically in ideal positions with a riding model, and all non-

hydrogen atoms were refined by the anisotropic thermal parameters during the final cycles. CCDC 2120700 and 2232465 contains the crystallographic data for this paper.

Chemicals

$CdCl_2 \cdot 2H_2O$, $CdBr_2 \cdot 2H_2O$, $ZnBr_2 \cdot 2H_2O$ and Bis-1-Thiophen-3-ylmethyl-[4,4'] bipyridinyl (Btybipy) were supplied by Macklin Reagent Co., Ltd. Mercury nitrate and other metal salts were all purchased from Kelong Reagent Co., Ltd. All organic reagents were bought from RunZe Reagent Co., Ltd.

Contents:

corresponding linear relationship between the fluorescence intensity of I/I_0 and Hg^{2+} concentration.

Fig. S9. (a) Fluorescence emission spectra of complex **1** in PBS buffer solution. (b) The corresponding linear relationship between the fluorescence intensity of I/I_0 and Hg^{2+} concentration.

Fig. S10. (a), (d) Fluorescence emission spectra of complexes **2–3** in PBS buffer solution. (b), (c), (e) and (f) The corresponding linear relationship between the fluorescence intensity of I/I_0 and Hg^{2+} concentration.

Fig. S11. CIE chromaticity diagram of complex **2** in the presence of different concentrations of Hg^{2+} from 0 to 400 μM.

Fig. S12. CIE chromaticity diagram of complex **3** in the presence of different concentrations of Hg^{2+} from 0 to 400 μM.

Fig. S13. Photographs of the corresponding color of the system treated with various cations. **(a)** under natural light and **(b)** 365 nm UV light.

Fig. S14. (a) Comparison of the ratiometric emission intensity I/I_0 for complex **2** treated with various cations. (1 mM) (b) Anti-interference experiment of complex **2** (100 μM Hg^{2+}).

Fig. S15. (a) Comparison of the ratiometric emission intensity I/I_0 for complex **3** treated with various cations. (1 mM) (b) Anti-interference experiment of complex **3** (100 μM Hg^{2+}).

Fig. S16. XPS survey spectra of complex **2** before and after treatment by Hg^{2+}.

Table S1. Crystal data and structure refinement for complexes **1–2**.

Table S2. Bond lengths [Å] and angles [°] for complexes **1**–**2**.

Table S3. Comparison of the Hg^{2+} detection properties of complexes with others methods reported in previous literature.

Table S4. Determination of Hg^{2+} in real water samples by complex **2**.

Table S5. Determination of Hg^{2+} in real water samples by complex **3**.

References

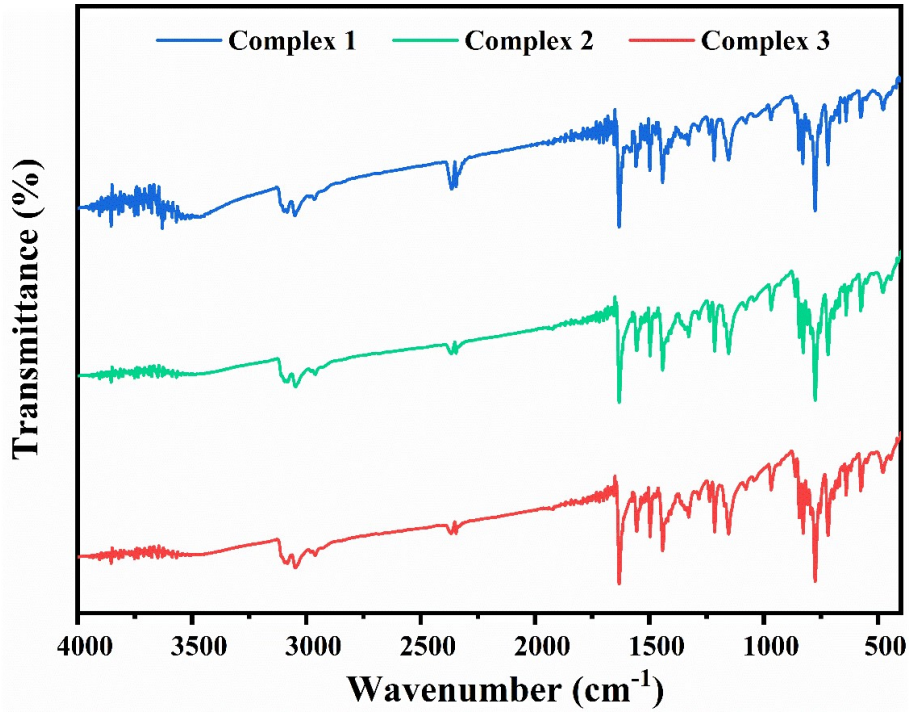

Fig. S1 FT-IR pattern of complexes **1–3**.

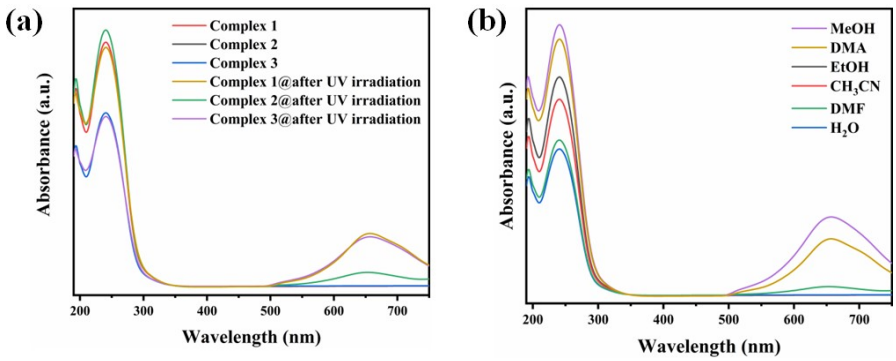

Fig. S2. UV-vis spectra of complexes **1–3:** (a) before and after UV irradiaton; (b) different solvent.

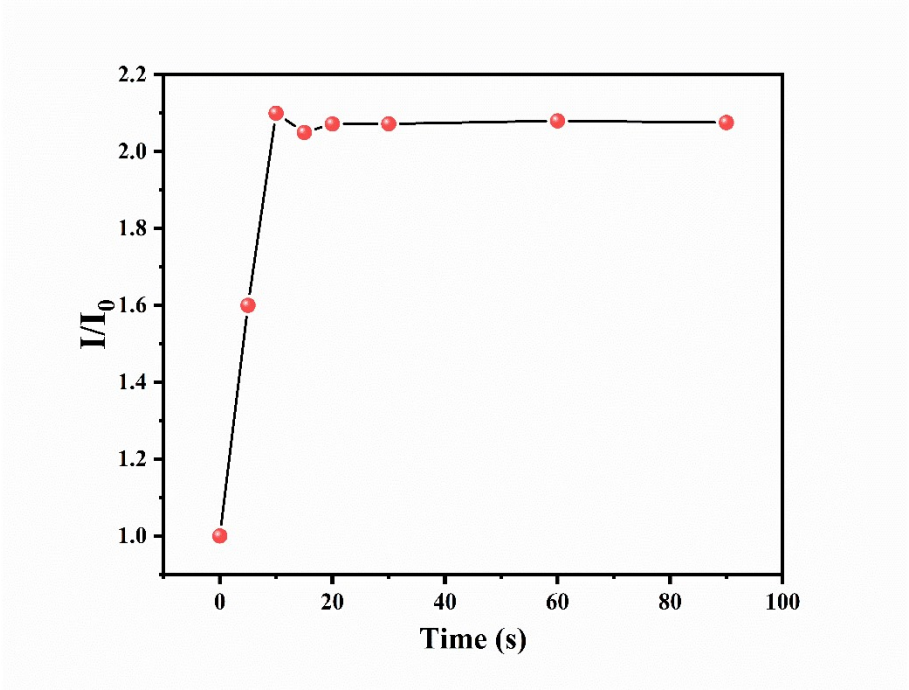

Fig. S3 Time-dependent fluorescence intensity of complex **1** suspension of Hg^{2+} aqueous dispersion in PBS buffer solution**.**

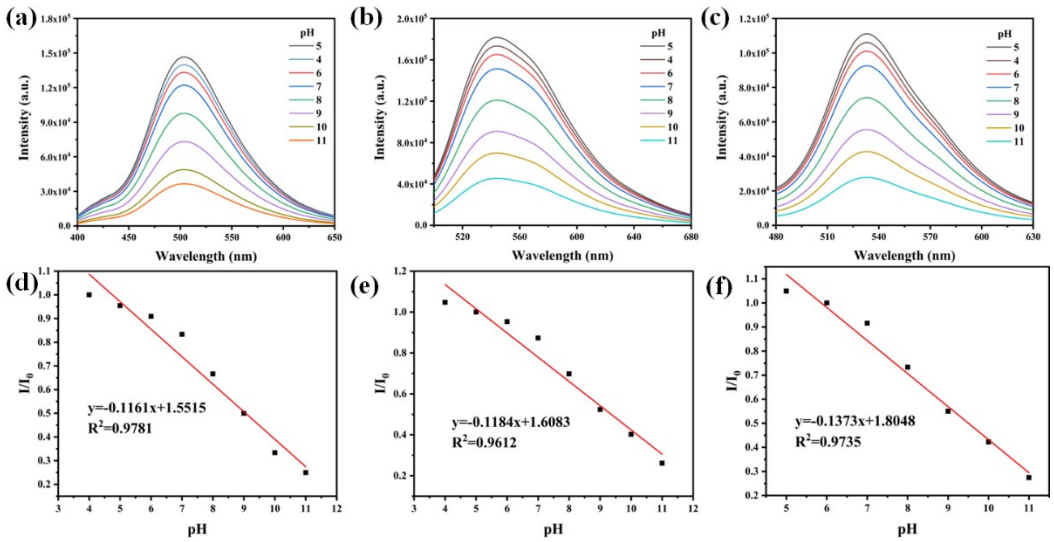

Fig. S4 Fluorescence emission spectra of pH values of complexes in PBS buffer solution: (a) complex **1**, (b) complex **2**, (c) complex **3.** The corresponding linear relationship between the fluorescence intensity of complexes and pH values: (d) complex **1**, (e) complex **2**, (f) complex **3**.

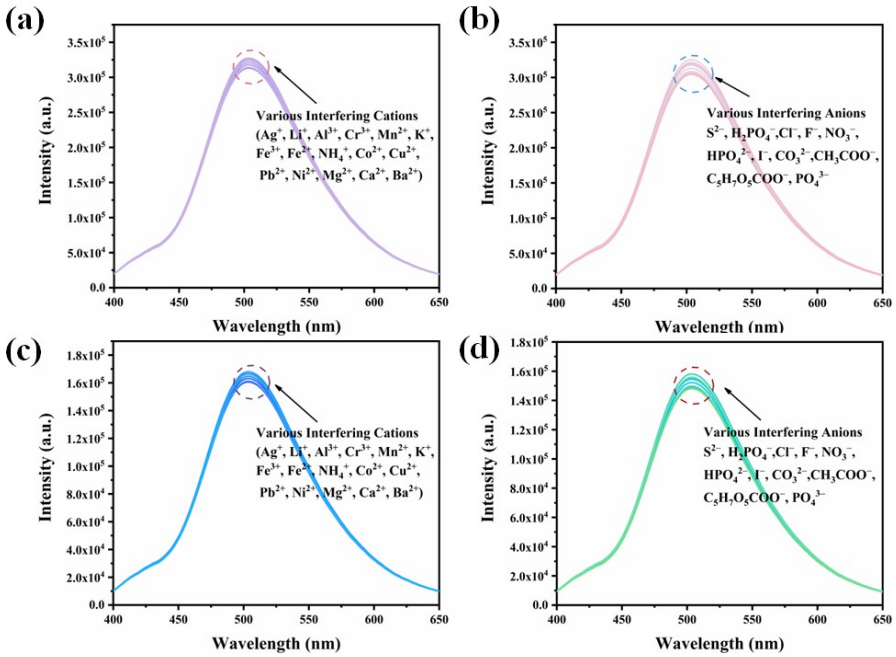

Fig. S5 Fluorescence emission spectra of complex **1** with various interfering ions in methanol solution: (a) cations, (b) anions. Fluorescence emission spectra of complex **1** with various interfering ions in PBS buffer solution: (c) cations, (d) anions.

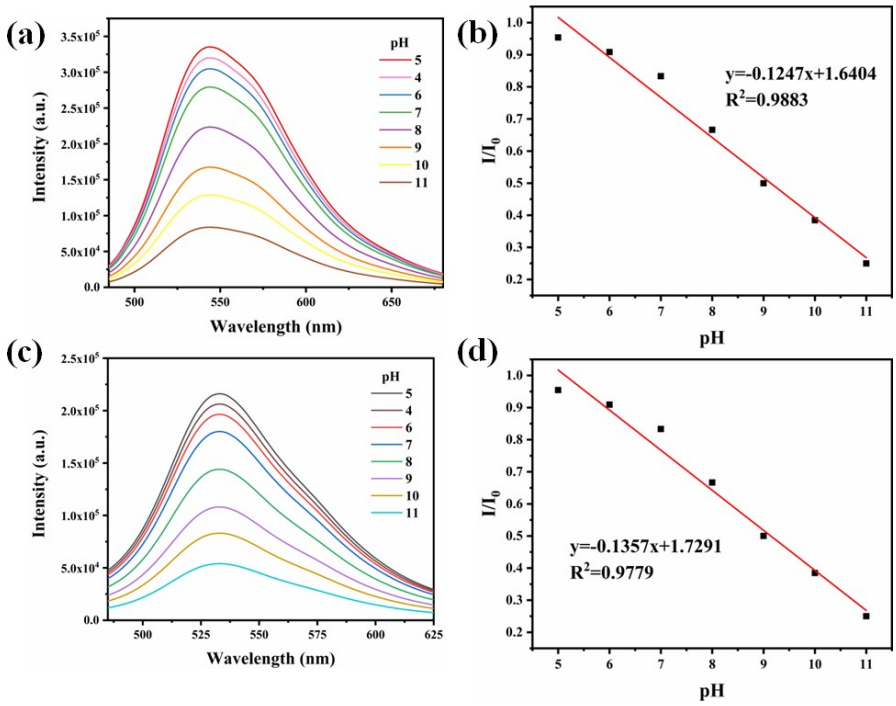

Fig. S6 Fluorescence emission spectra of pH values of complexes in methanol solution. (a) complex **2**, (c) complex **3.** The corresponding linear relationship between the fluorescence intensity of complexes and pH values. (b) complex **2**, (d) complex **3**.

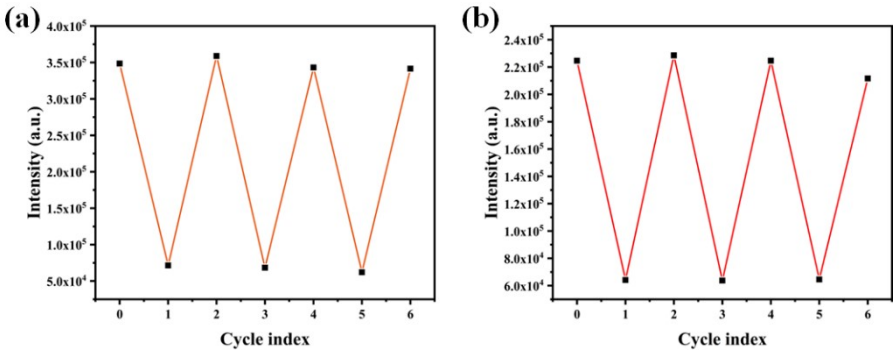

Fig. S7 Changes in fluorescence of complexes **2–3** under cyclic treatment of Hg^{2+}.

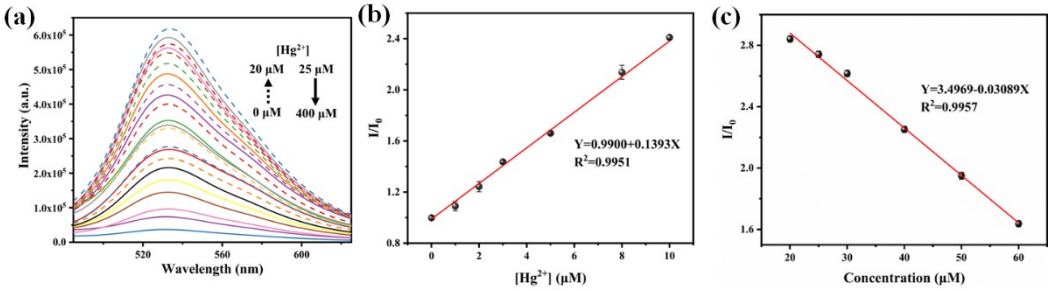

Fig. S8 (a) Fluorescence emission spectra of complex **3** in methanol solution. (b), (c)The corresponding linear relationship between the fluorescence intensity of I/I_0 and Hg^{2+} concentration.

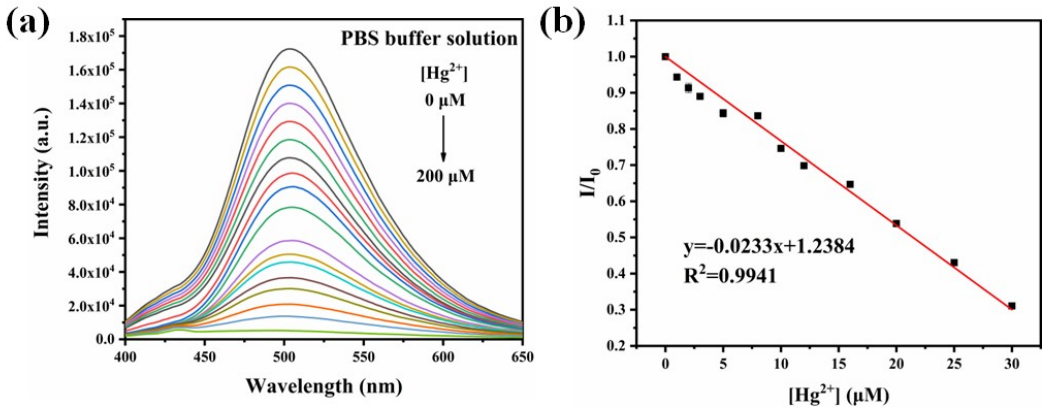

Fig. S9 (a) Fluorescence emission spectra of complex **1** in PBS buffer solution. (b) The corresponding linear relationship between the fluorescence intensity of I/I_0 and Hg^{2+} concentration.

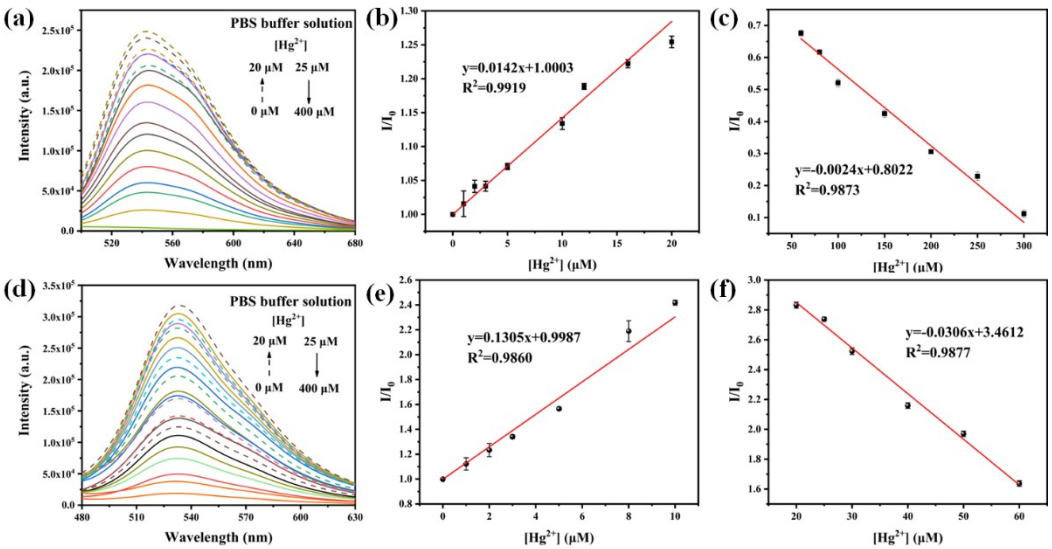

Fig. S10 (a), (d) Fluorescence emission spectra of complexes **2–3** in PBS buffer solution. (b), (c), (e) and (f) The corresponding linear relationship between the fluorescence intensity of I/I_0 and Hg^{2+} concentration.

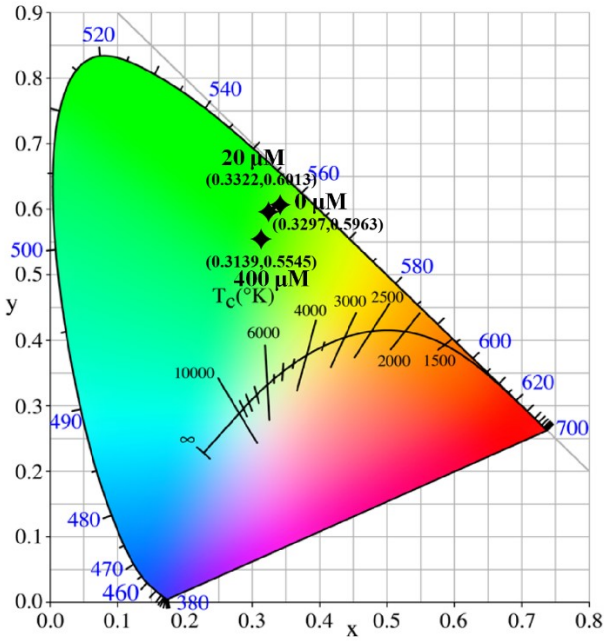

Fig. S11 CIE chromaticity diagram of complex **2** in the presence of different concentrations of Hg^{2+} from 0 to 400 μM.

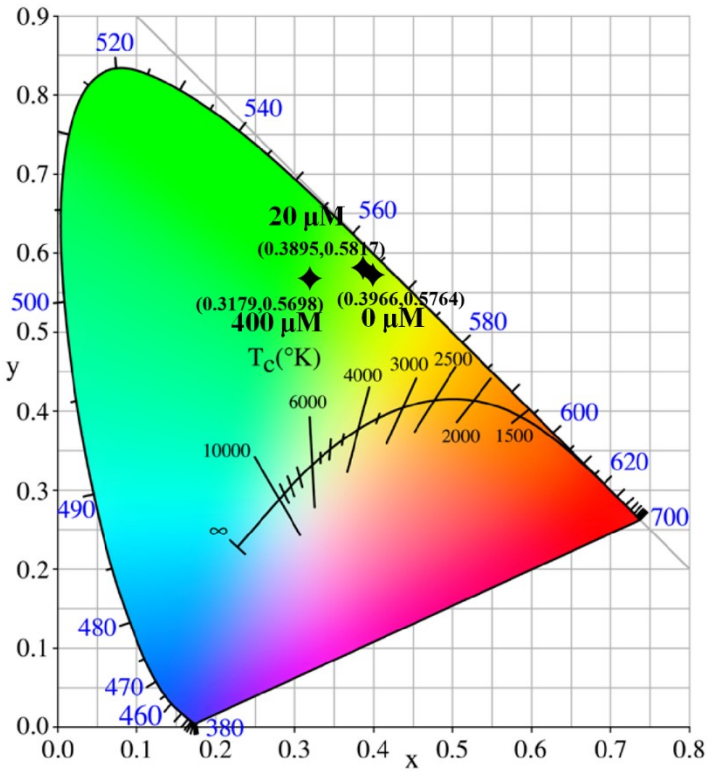

Fig. S12 CIE chromaticity diagram of complex **3** in the presence of different concentrations of Hg^{2+} from 0 to 400 μM.

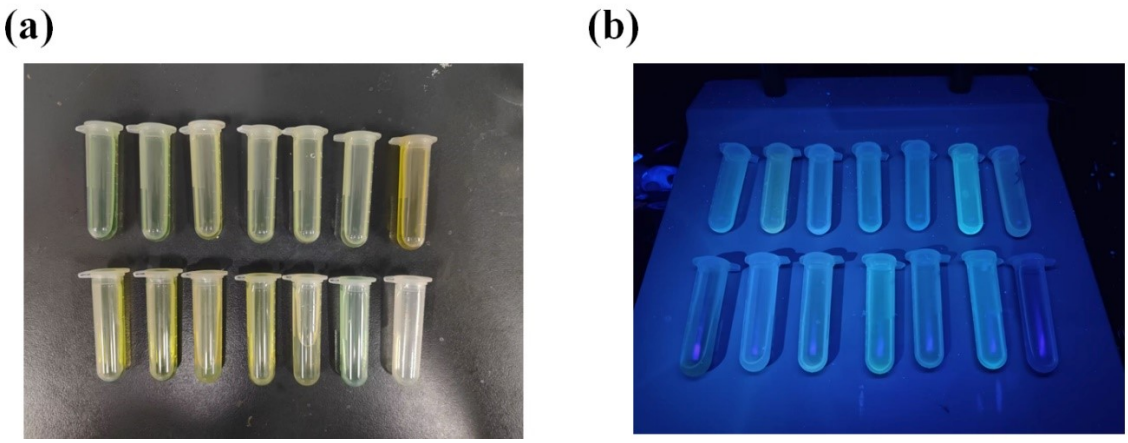

Fig. S13 Photographs of the corresponding color of complex **1** system treated with various cations. **(a)** under natural light and **(b)** 365 nm UV light.

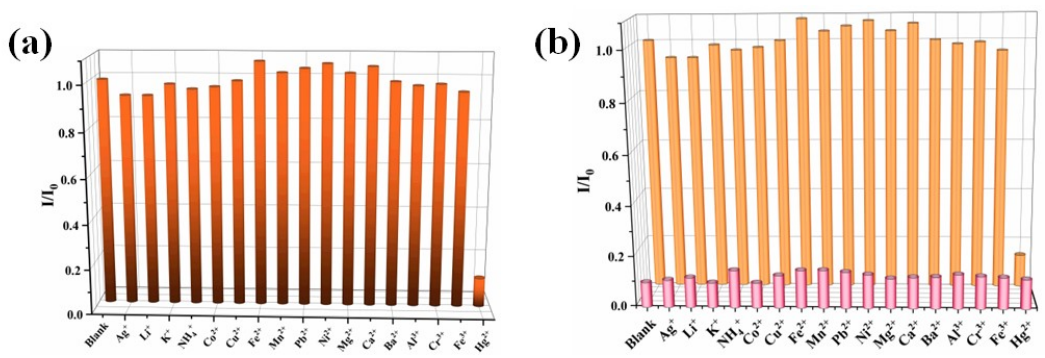

Fig. S14 (a) Comparison of the ratiometric emission intensity I/I_0 for complex **2** treated with various ions (1 mM). (b) Anti-interference experiment of complex **2** (100 μM Hg^{2+}).

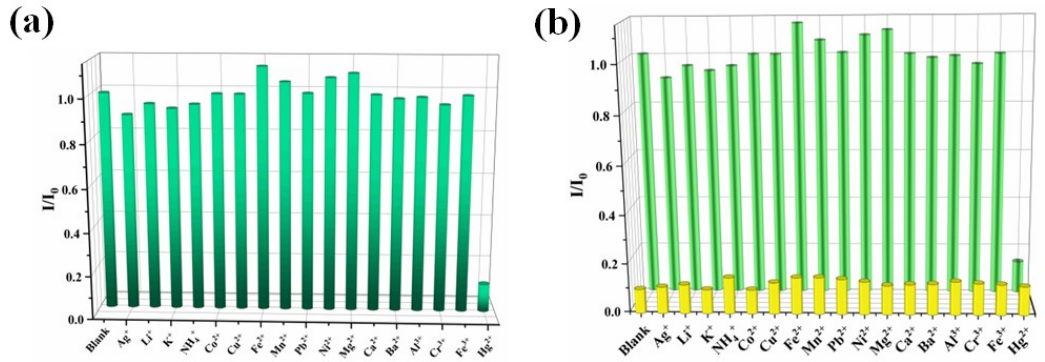

Fig. S15 (a) Comparison of the ratiometric emission intensity I/I_0 for complex **3** treated with various ions (1 mM). (b) Anti-interference experiment of complex **3** (100 μM Hg^{2+}).

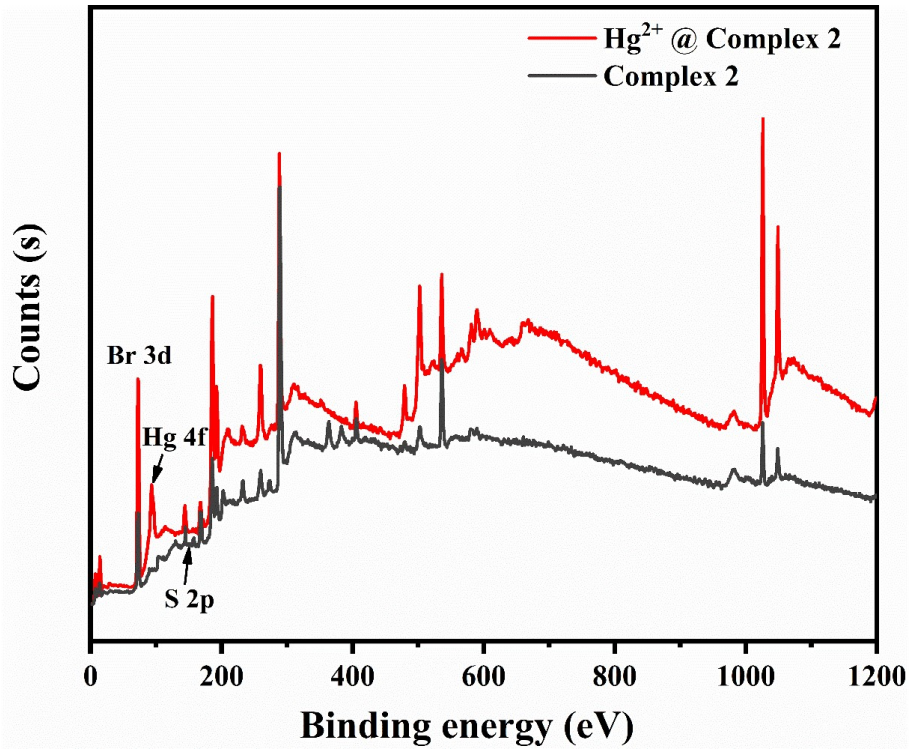

Fig. S16 XPS survey spectra of complex **2** before and after treatment by Hg^{2+}.

Table S1 Crystal data and structure refinement for complexes **1–2**.

	1	**2**
Empirical formula	$C_{20}H_{18}CdCl_4N_2S_2$	$C_{20}H_{18}ZnBr_4N_2S_2$
Formula weight	604.69	735.47
Crystal system	orthorhombic	orthorhombic
Space group	$P2_12_12_1$	$P2_12_12_1$
a/Å	8.7427(4)	8.6729(4)
b/Å	15.4914(7)	16.0066(8)
c/Å	17.1013(7)	17.1150(8)
α/°	90	90
β/°	90	90
γ/°	90	90

Volume/Å^3	2316.14(18)	2376.0(2)
Z	4	4
D_c (g×cm^{-3})	1.734	2.056
μ/mm^{-1}	1.595	7.947
F(000)	1200.0	1416.0
R_1[a] [I > 2σ(I)]	0.0580	0.0388
wR_2[b] (all data)	0.1657	0.0829
GOF on F^2	1.074	1.025

[a] $R^1 = \Sigma||F_o|-|F_c||/\Sigma|F_o|$; [b] $wR^2 = [Sw(F_o^2-F_c^2)^2/Sw(F_o^2)^2]^{1/2}$.

Table S2. Bond lengths [Å] and angles [°] for complexes **1**–**2**.

Complex **1**			
Br(1)-Zn(1)	2.4135(14)	N(2)-C(8)	1.315(12)
Zn(1)-Br(4)	2.388(3)	S(1)-C(15)	1.683(11)
S(2)-C(1)	1.81(2)	N(1)-C(7)	1.342(12)
Br(2)-Zn(1)-Br(1)	109.40(6)	Br(3)-Zn(1)-Br(1)	111.46(6)
Br(3)-Zn(1)-Br(2)	106.46(6)	Br(4)-Zn(1)-Br(3)	115.47(15)
C(15)-S(1)-C(20)	92.5(5)	C(17)-S(2)-C(1)	102.1(9)
C(4)-N(1)-C(7)	120.0(8)	C(13)-N(2)-C(18)	118.3(8)
Complex **2**			
Cd(1)-Cl(1)	2.486(3)	Cd(1)-Cl(2)	2.462(3)
Cd(1)-Cl(3)	2.479(4)	S(1)-C(1)	1.706(17)
S(2)-C(15)	1.689(18)	N(1)-C(4)	1.356(15)
Cl(2)-Cd(1)-Cl(1)	109.21(11)	Cl(2)-Cd(1)-Cl(3)	108.62(12)
Cl(2)-Cd(1)-Cl(4)	112.81(16)	Cl(3)-Cd(1)-Cl(4)	100.93(18)
C(11)-S(1)-C(1)	96.7(8)	C(17)-S(2)-C(15)	92.0(8)
C(4)-N(1)-C(7)	119.1(10)	C(12)-N(2)-C(16)	117.7(11)

Table S3. Comparison of the Hg^{2+} detection properties of complexes with others methods reported in previous literature.

Methods	Materials	Linear range (μM)	Detection Limits (nM)	References
Fluorescence	Ru@UiO-66-NH_2	0-200	53	[S1]
Fluorescence	CDs-Rho	0-100	2.91	[S2]
Fluorescence	AH-COF	0-40	100	[S3]
Fluorescence	Eu-Ca-MOF	0.02-200	2.6	[S4]
Fluorescence	Probe 1	0-10	21.6	[S5]
Fluorescence	Complex **1**	0-30	3.11	This work
Fluorescence	Complex **2**	0-10 20-60	2.14	This work
Fluorescence	Complex **3**	0-20 50-300	3.13	This work

Table S4. Determination of Hg^{2+} in real water samples by complex **2** (n=3).

Sample	**Hg^{2+}spiked (μM/L)**	**Detect Hg^{2+} (μM /L) Mean±SD**	**Recovery (%)**	**RSD (%)**
Tap water	0	/	/	/
	2	1.92	95.85	0.66
	4	4.04	101.10	1.49
	8	8.1	101.20	0.89
	16	16.05	100.30	1.54
Lake water	0	/	/	/

	2	1.95	97.30	2.48
	4	3.99	99.70	2.16
	8	7.97	99.60	1.44
	16	16.20	101.20	1.58

Table S5 Determination of Hg^{2+} in real water samples by complex **3** (n=3).

Sample	**Hg^{2+}spiked (μM /L)**	**Detect Hg^{2+} (μM /L) Mean±SD**	**Recovery (%)**	**RSD (%)**
Tap water	0	/	/	/
	2	1.97	98.40	1.56
	4	4.05	101.33	2.02
	8	8.03	100.33	1.21
	16	16.30	101.84	0.81
Lake water	0	/	/	/
	2	2.01	100.30	2.14
	4	4.03	100.63	1.98
	8	7.98	99.80	1.84
	16	15.90	99.40	1.11

References:

[S1]P. Jia, K.R. Yang, J.J. Hou, Y.Y. Cao, X. Wang and L. Wang, J Hazard. Mater.,

2020, **408**, 124469.

[S2]M. Li, X.N. Li, M.W. Xu, B.W. Liu, M.Q. Yang, Z.J. Chen, T.C. Gao, T.D. James, L.D. Wang and H.B. Xiao, Chem. Eng. J., 2021, 426, 131296.

[S3]Y.X. Yu, G.L. Lia, J.H. Liu and D.Q. Yuan, Chem. Eng. J., 2020, 401, 126139.

[S4]N.W.H. Guo, l.P. Peng, Y. Chen, Y.S. Liu, C.L. Li, H. Zhang and W. Yang, Talanta, 2022, 250, 123710.

[S5]X.M. Wu, Y.N. Li, S.X. Yang, H.Y. Tian and B.G. Sun, Microchem., 2020, 157, 105024.